4-Hydroxyacetophenone modulates the actomyosin cytoskeleton to reduce metastasis

Darren S. Bryan[a,1], Melinda Stack[a,1], Katarzyna Krysztofiak[b,c], Urszula Cichoń[b,d], Dustin G. Thomas[e], Alexandra Surcel[e], Eric S. Schiffhauer[e], Michael A. Beckett[f,g], Nikolai N. Khodarev[f,g], Lai Xue[a], Elizabeth C. Poli[a], Alexander T. Pearson[h], Mitchell C. Posner[a], Douglas N. Robinson[e], Ronald S. Rock[b,2], and Ralph R. Weichselbaum[f,g,2]

[a]Department of Surgery, The University of Chicago, Chicago, IL 60637; [b]Biochemistry and Molecular Biology, The University of Chicago, Chicago, IL 60637; [c]Faculty of Biology, University of Warsaw, 00-927 Warsaw, Poland; [d]Faculty of Biochemistry, Biophysics and Biotechnology, Jagiellonian University, 31-007 Kraków, Poland; [e]Department of Cell Biology, Johns Hopkins School of Medicine, Baltimore, MD 21205; [f]Department of Radiation and Cellular Oncology, The University of Chicago, Chicago, IL 60637; [g]The Ludwig Center for Metastasis Research, The University of Chicago, Chicago, IL 60637; and [h]Department of Medicine, The University of Chicago, Chicago, IL 60637

Edited by David J. DeRosier, Brandeis University, Waltham, MA, and approved August 5, 2020 (received for review July 13, 2020)

Metastases are the cause of the vast majority of cancer deaths. In the metastatic process, cells migrate to the vasculature, intravasate, extravasate, and establish metastatic colonies. This pattern of spread requires the cancer cells to change shape and to navigate tissue barriers. Approaches that block this mechanical program represent new therapeutic avenues. We show that 4-hydroxyacetophenone (4-HAP) inhibits colon cancer cell adhesion, invasion, and migration in vitro and reduces the metastatic burden in an in vivo model of colon cancer metastasis to the liver. Treatment with 4-HAP activates nonmuscle myosin-2C (NM2C) (*MYH14*) to alter actin organization, inhibiting the mechanical program of metastasis. We identify NM2C as a specific therapeutic target. Pharmacological control of myosin isoforms is a promising approach to address metastatic disease, one that may be readily combined with other therapeutic strategies.

colorectal cancer | nonmuscle myosin 2C | 4-hydroxyacetophenone | ex vivo motility | metastasis

Metastatic disease contributes to 90% of cancer related deaths (1, 2). Treatment strategies for metastatic cancer vary depending on the histological type, extent, and aggressiveness of disease. In one treatment paradigm, metastatic disease is prevented and micrometastatic disease eliminated through adjuvant therapy following treatment of the primary tumor. In patients who develop or present with limited metastatic disease, localized ablative therapies, such as surgery or radiation may be curative (3). However, most patients require systemic treatment with chemotherapy, immunotherapy, hormonal therapy, or treatment with small molecule inhibitors. Regardless of the therapeutic regimen, progression of disease may occur, either from seeding of new metastasis by established metastatic colonies, or recurrence of the primary tumor from local growth or reseeding by circulating tumor cells (4, 5). Therefore, new treatment strategies that target the initial development of metastatic disease and the progression of metastatic disease are needed (6).

Cell migration to favored environments is an evolutionarily conserved behavior that can be observed in single cells, developmental processes in model organisms, and in patterns of metastatic cancer progression (7). Malignant cells that gain metastatic potential develop a more motile and invasive phenotype, allowing for disease progression (8–10). For cells to disseminate from the primary tumor and undergo intravasation to the systemic circulation, they must remodel their actomyosin cytoskeleton and increase their deformability (11). Cells must also tolerate shear stress encountered while circulating to end organs, before arresting and adhering to a distant vessel. Eventually, cells again adopt a deformable conformation to extravasate, invade, and migrate to establish a distant metastatic colony (11–13). Pharmacologic targeting of this mechanical program is, therefore, of great interest (6, 14).

Attempts to inhibit upstream regulatory pathways that control actomyosin contractility have failed to generate clinically effective therapies. Actomyosin regulation involves multiple redundant signaling pathways that provide routes for therapy resistance (15–17). A promising approach to circumvent development of resistance is to target the final outputs of the signaling pathway, such as the molecular machines themselves (14, 18). Nonmuscle myosin-2 (NM2) is one such machine that establishes cellular directional polarity, mediates integrin-associated adhesion, and is key in the maturation and elongation of cellular protrusions (lamellipodia) that drive migration (19–22). Importantly, NM2 lies at the endpoint of multiple upstream signaling pathways, primarily Rho-associated GTPases, and represents a specific target for therapy as indicated in a glioma model system (18).

The small molecule 4′-hydroxyacetophenone (4-HAP) activates nonmuscle myosin-2B (NM2B, *Myh10*) and -2C (NM2C, *Myh14*) by promoting their assemblies (23). Here, we demonstrate that 4-HAP decreases metastatic burden in an in vivo model system of colorectal cancer liver metastases. Treatment with 4-HAP remodels actin through a M2C-dependent process

Significance

There is a pressing need for new approaches to combat metastatic disease. We demonstrate, here, a strategy that targets and activates the molecular machines that control cell shape in cell division, wound healing, immune surveillance, embryonic development, and cancer metastasis. Cells control their shape by remodeling their cytoskeletal actin filaments, microtubules, and intermediate filaments, while cytoskeletal motor proteins, such as the myosins generate forces that can produce local contractions. By targeting and activating NM2C directly, we interfere with cytoskeletal plasticity. We demonstrate the effectiveness of this activation strategy *in vitro* and *in vivo* and provide a molecular mechanism for our measured increase in cell stiffness. Our strategy can be integrated readily with existing approaches to combat aggressive cancers.

Author contributions: D.S.B., M.S., K.K., U.C., A.S., M.A.B., M.C.P., D.N.R., R.S.R., and R.R.W. designed research; D.S.B., M.S., K.K., U.C., D.G.T., A.S., E.S.S., M.A.B., N.N.K., and L.X. performed research; D.G.T., D.N.R., R.S.R., and R.R.W. contributed new reagents/analytic tools; D.S.B., M.S., K.K., U.C., A.S., M.A.B., E.C.P., A.T.P., and R.S.R. analyzed data; and D.S.B., R.S.R., and R.R.W. wrote the paper.

The authors declare no competing interest.

This article is a PNAS Direct Submission.

[1]D.S.B. and M.S. contributed equally to this work.

[2]To whom correspondence may be addressed Email: rrock@uchicago.edu or rrw@radonc.uchicago.edu.

This article contains supporting information online at https://www.pnas.org/lookup/suppl/doi:10.1073/pnas.2014639117/-/DCSupplemental.

First published August 26, 2020.

and ultimately blocks the ability of the cells to polarize, disseminate, and invade. A recent report by Surcel shows that 4-HAP has similar effects on metastasis in pancreatic cancer model systems (24). Because the pancreatic cancer cells express only NM2C while the colon cancer cells express both NM2B and NM2C, our work in this colon cancer model shows that NM2C is the major target for 4-HAP's antimetastatic activity (24). Together, these data demonstrate that modulation of the actomyosin cytoskeleton is a viable target for future cancer therapeutics in the context of suppressing metastatic spread and could be combined with current therapeutics.

Results

4-HAP Limits Cell Adhesion, Invasion, and Migration. We evaluated the effect of 4-HAP on the human colorectal cancer cell line HCT116. We performed proliferation assays, demonstrating a modest dose-dependent decrease in cellular proliferation in the presence of 4-HAP from 0 to 4 μM. At all concentrations, cell division continues to occur, however, at lower rates with higher concentrations of 4-HAP. After 72 h at the highest concentration of 4 μM, the cell count as measured by a fluorescence assay decreases by 23% (Fig. 1*A*). Taken together, these experiments suggest that, at low μM concentrations, 4-HAP is not cytotoxic. We next performed cell adhesion, invasion, and migration assays in the presence of increasing concentrations of 4-HAP, again using a maximum concentration of 4 μM. Wild type HCT116 cells treated with all concentrations of 4-HAP show a significant dose-dependent decrease in adhesion, invasion, and migration, with migration the most strongly inhibited of the three (Fig. 1 *B–D*).

Our prior work has shown that 4-HAP affects the assembly of NM2B and NM2C (23). We, therefore, measured the concentration of NM2s in our HCT116 cells using quantitative Western analysis. NM2A (*MYH9*) is the dominant isoform, but NM2B (*MYH10*) and NM2C (*MYH14*) (23) are both present at 4–6% of the total (*SI Appendix*, Fig. S1*A*). Next, we generated a HCT116 cell line in which NM2C expression was reduced by 60% (short hairpin NM2C [shNM2C], see *SI Appendix*, Fig. S1*B*) using lentiviral-based RNA interference. We repeated the proliferation experiments on the shNM2C cells and found that the shNM2C grew more slowly than wild type and that the growth rate was insensitive to 4-HAP (Fig. 1*E*). We repeated the adhesion, invasion, and migration assays with shNM2C knockdown cells and found that all three cell behaviors are largely unaffected by 4-HAP (Fig. 1 *F–H*). From these knockdown experiments, we conclude that 4-HAP inhibits in vitro adhesion, invasion, and migration largely through NM2C activity.

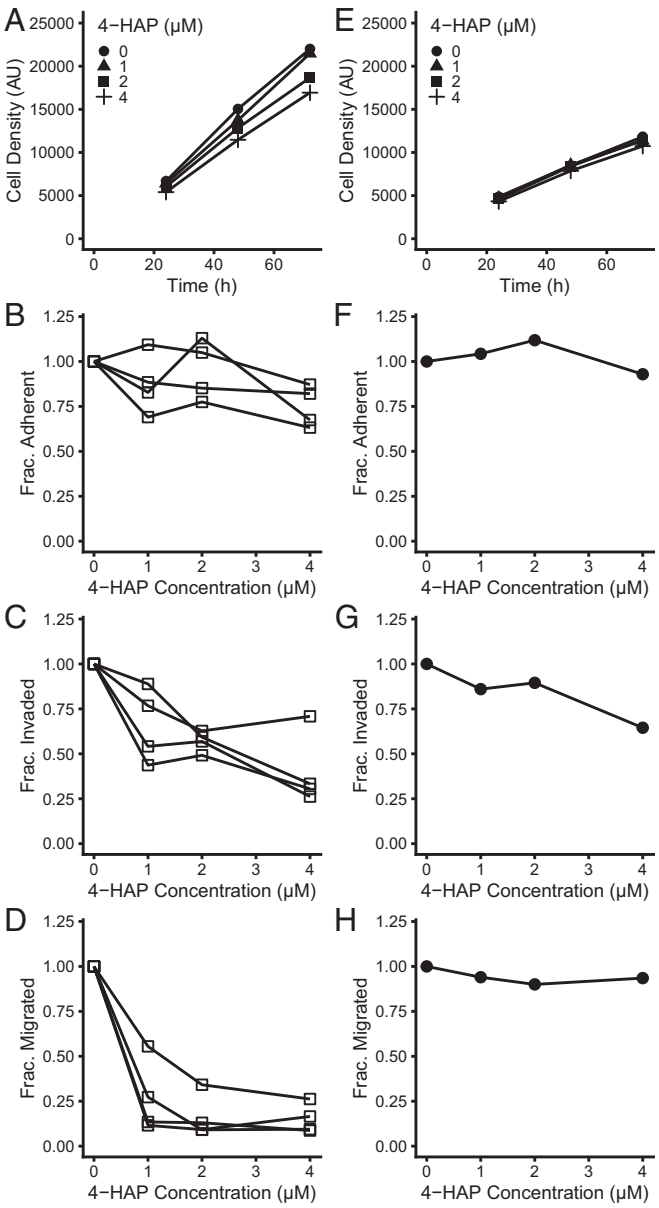

Fig. 1. The compound 4-HAP limits cellular adhesion, invasion, and migration in a dose-dependent fashion. (*A*) Treatment with 4-μM 4-HAP leads to a modest 23% decrease in cell density at 72 h. The dose-dependent proliferation defect as determined by the interaction of time and concentration is statistically significant ($P = 0.001$). We observe a statistically significant dose-dependent decrease in (*B*) adhesion ($P = 0.03$), (*C*) invasion ($P = 0.0002$), and (*D*) migration ($P = 0.002$). In HCT116 cells knocked down for myosin NM2C, we found no significant dose-dependent differences in (*E*) proliferation ($P = 0.3$), (*F*) adhesion ($P = 0.6$), (*G*) invasion ($P = 0.06$), or (*H*) migration ($P = 0.4$). For all panels, each point represents the mean of three technical replicates, and each line represents an independent biological replicate. We used linear regression of the biological replicates to obtain *P* values for zero slopes or interactions using an α level of 0.05 to determine significance.

4-HAP Limits the Development and Spread of Metastases In Vivo. Using a previously described model of liver metastasis, we performed splenic injections with HCT116 cells, dual labeled with TdTomato and luciferase (25). By injecting the spleen, the portal circulation feeding the liver was seeded with 1.5×10^6 tumor cells, establishing liver tumor colonies and simulating metastases. Mice underwent pretreatment with 1 mg/kg 4-HAP (treatment) or phosphate-buffered saline (PBS) (control) for 3 d prior to splenic injection with daily redosing for 4 wk. Using bioluminescent imaging, we monitored tumor growth in the mice over a period of 4 wk. Treatment with 4-HAP halves the tumor growth rate from 6.0 ± 1.2/wk to 3.0 ± 0.8/wk (Fig. 2 *A–C*, ± SE, χ^2 [1] = 7.65, $P = 0.006$). When the experiment was repeated with shNM2C knockdown HCT116 cells, liver metastases grow at 6.8 ± 2.6/wk, and the rate is not significantly altered in the mice treated with 4-HAP (Fig. 2 *D–F*, ± SE, χ^2 [1] = 0.20, $P = 0.65$). This unchanged rate is consistent with 4-HAP acting through NM2C.

Because 4-HAP treatment reduces the mechanical processes of adhesion, invasion, and migration in vitro and metastatic load in vivo, we next investigated the mechanism by which 4-HAP affects cell mechanics. As 4-HAP is a M2 activator and is expected to contract actin filaments, we focused our attention on cellular stiffness and actin filament density and organization. In these mechanistic studies, we seek effects that are mediated by NM2C because NM2C has the dominant role in the metastatic events shown in Figs. 1 and 2.

Treatment with 4-HAP Increases Cortical Tension of HCT116 Cells but Not through NM2C. One useful global measure of the cell mechanics is the cortical tension (T_{eff}), which defines an energetic

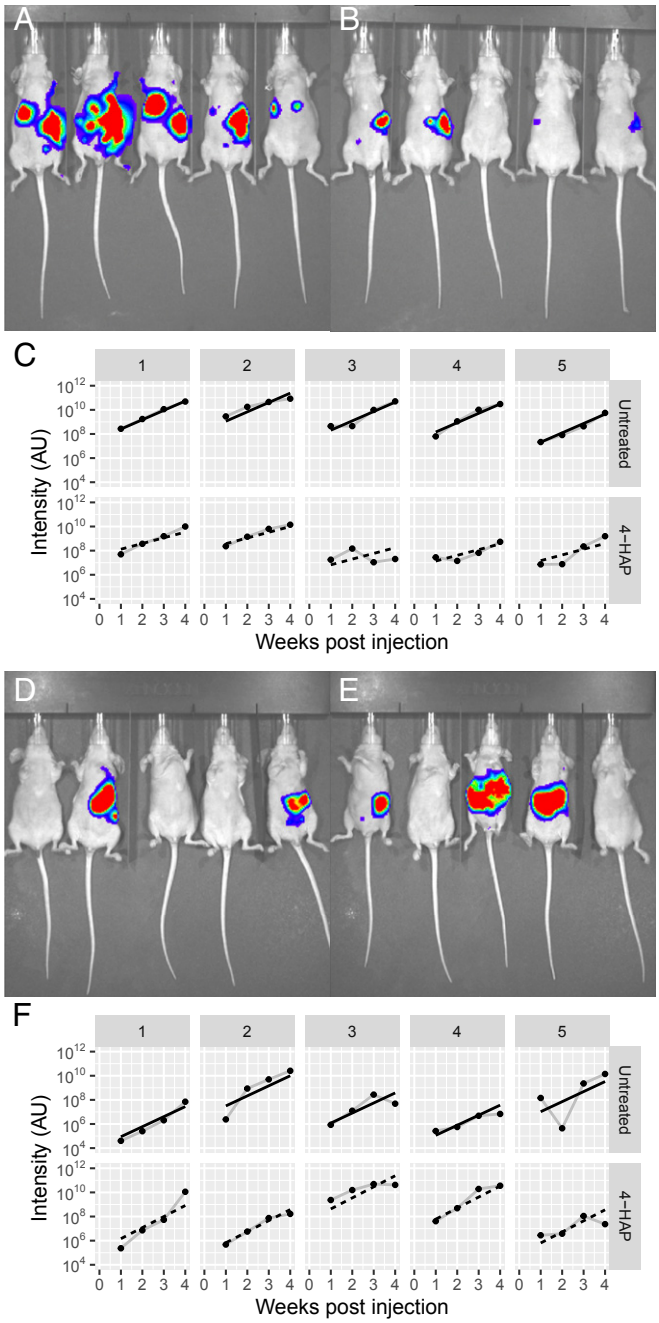

Fig. 2. Treatment with 4-HAP limits the development and spread of metastases in vivo. At the end of 4 wk, tumor burden in (*A*) athymic *nude* mice injected with HCT116 cells was greater than in (*B*) mice treated with 4-HAP. (*C*) Intensity traces of the individuals shown in (*A* and *B*) over the 4-wk period. Trend lines show exponential growth modeled as a fixed rate across each treatment with individual (random effect) intercepts for each subject (conditional $R^2 = 0.86$). Treatment with 4-HAP significantly decreases the apparent tumor growth rate from 6.0 ± 1.2/wk to 3.0 ± 0.8/wk (±SE, χ^2 [1] = 7.65, and $P = 0.006$). Mice injected with shNM2C knockdown HCT116 cells (*D* and *E*) demonstrated no significant difference in exponential tumor growth rate when treated with 4-HAP (*F*, 6.8 ± 2.6/wk, ±SE, χ^2 [1] = 0.20, $P = 0.65$, and conditional $R^2 = 0.81$). Note that these mice start at a lower initial tumor mass compared to those injected with wild type HCT116 cells, which likely reflects a seeding defect from the NM2C knockdown itself.

cost of increasing the cell's surface area. The cortical tension includes contributions from passive elasticity and active cytoskeleton-generated tension from both actin polymer assembly and M2-mediated contractility. Because motile cells continuously adjust their shapes, this energic cost for shape deformation can impede motility.

We measured the cortical tension of untreated and 4-HAP-treated HCT116 cells using micropipette aspiration where pressure is externally applied to measure deformability. Example images of the aspirated cells are shown in Fig. 3*A*. The untreated cells have a moderate cortical tension of 0.5 nN/μm (Fig. 3*B*), which is comparable with many other cell types including HL-60 cells (0.3 nN/μm) and *Dictyostelium discoideum* cells (0.8–1 nN/μm) (23, 26). When treated with 500-nM 4-HAP, the HCT116 cells would often bleb into the pipette before they distort by a measurable amount (Fig. 3*A*, arrow). When such blebbing occurs, T_{eff} cannot be measured due to the dissociation of the plasma membrane from the actomyosin cytoskeleton. We compensated by reducing the rate at which the cells were aspirated, which suppressed this blebbing phenomenon. Treatment with 4-HAP increases the cortical tension by ∼0.1 nN/μm in wild type short hairpin control (shCtrl) cells (Fig. 3*B*). Knockdown of NM2C reduced the cortical tension, however, the increase in tension upon 4-HAP treatment was the same ∼0.1 nN/μm (Fig. 3*B*). Thus, 4-HAP increases cortical tension through a different target, which is likely NM2B rather than NM2C.

HCT116 Cells Have Numerous Actin Projections but No Stress Fibers. Having excluded increased cortical tension as the explanation for 4-HAP's antimestatic activity, we next turned to a detailed examination of the actin architecture in HCT116 cells. In general, motors, such as M2 construct and operate on actin structures a mixed filament polarity so that bipolar filaments of NM2 can reel in the pointed ends of actin into a stable load-bearing structure. One common example of a contractile actin structure in nonmuscle cells are the stress fibers, which are long bundles of actomyosin and associated cytoskeletal proteins (27). Cortical actin at the plasma membrane is also of mixed polarity and contracts due to the motor activity of embedded NMs. In other regions of uniform actin polarity in the cell, bipolar filaments move along the actin without contraction of the actin itself (28).

To identify contractile actin structures, we imaged HCT116 cells on polylysine-coated coverslips and stained with tetramethylrhodamine (TMR)-phalloidin for actin and immunostained for NM2C (Fig. 3*C*). The HCT116 cells are uniformly round with numerous thin projections at the periphery that resemble filopodia and lack stress fibers (27). The NM2C appears in a punctate pattern across the actin cortex with more NM2C in the central zone, although a few NM2C puncta are observed in the apparent filopodial structures. Cells treated with 4-HAP have a similar overall actin architecture, lacking obvious contractile structures, such as stress fibers. Moreover, treatment with 4-HAP does not grossly affect the localization of NM2C in single HCT116 cells.

Myosin Motor Tracking Reveals Mixed Polarity Actin Networks. Because conventional epifluorescence microscopy cannot resolve individual actin filaments, we next turned to a high-resolution functional imaging approach to map the organization of the actin networks in these cells. In our ex vivo motility assay (29), we track fluorescent-labeled processive myosin motors as in conventional in vitro motility, but instead of using purified actin filaments as tracks, we expose the actin networks in cultured cells by opening them with detergent (30). We, then, apply fluorescent myosin molecules, track single myosins as they travel along the cellular actin, and record a map of the myosin trajectories. We use two processive motors, the barbed-end-directed myosin-5 (M5) and pointed-end-directed myosin-6 (M6), which allows us to assess the overall organization of actin filament orientation. Furthermore, these two myosins differ in their actin track preferences. For example, M5 travels farther and lands at a higher rate on young actin filaments, while M6 has the opposite preference

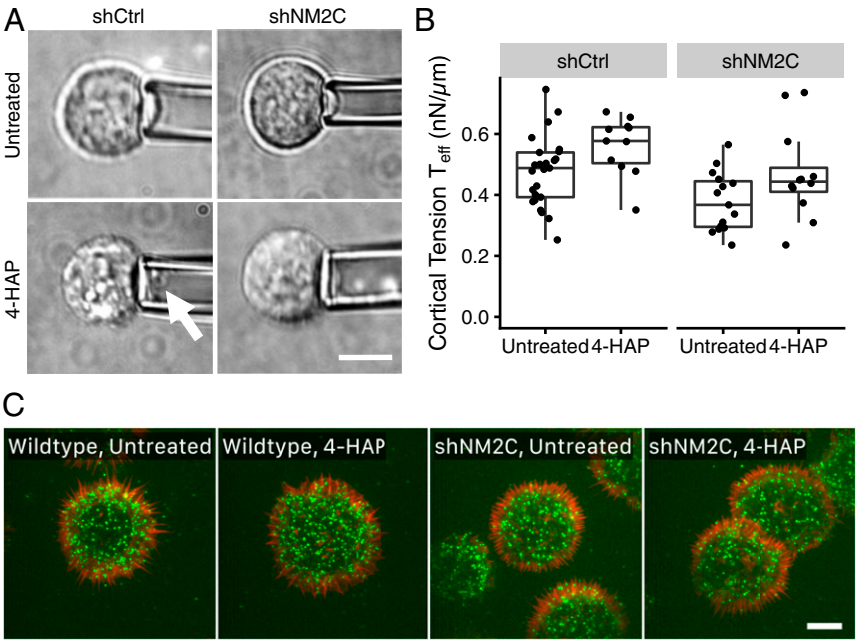

Fig. 3. NM2C activated with 4-HAP does not contribute to cortical tension and does not redistribute in HCT116 cells. (*A*) Micrographs showing micropipette aspiration of HCT116 cells. Wild type (shCtrl) or NM2C knockdown cells (shNM2C) were aspirated ±500 nM 4-HAP. Under standard aspiration rates, shCtrl cells treated with 4-HAP stiffened to an extent that the membrane-cortex connection ruptures and the cells form blebs in the pipette (arrow). We, therefore, reduced the aspiration rate for shCtrl cells to prevent this blebbing. (*B*) Cortical tension measurements. Cortical tension increased by 0.09 ± 0.03 nN/μm upon treatment with 4-HAP (±SE, $F[1, 60] = 8.27$, and $P = 0.006$) and decreased by 0.1 ± 0.03 nN/μm in shNM2C cells (±SE, $F[1, 60] = 11.0$, and $P = 0.002$). However, no significant interaction was observed between treatment and strain ($F[1, 59] = 0.006$ and $P = 0.94$). This lack of interaction suggests that 4-HAP modulates cortical tension through a different target in HCT116 cells, likely NM2B. (*C*) Treatment with 4-HAP does not affect NM2C localization. Total internal reflection fluorescence microscopy images of HCT116 cells stained for NM2C (green) and actin (red) show a punctate NM2C staining pattern. The NM2C is found uniformly distributed in the central region of the cell behind an actin-rich band containing many apparent filopodia, although a few NM2C puncta appear in the filopodia as well. As expected, fewer NM2C puncta are seen in the shNM2C cells. (Scale bars, 5 μm.)

for old actin filaments (31). Because actin subunit age within a filament is recorded by its nucleotide state, and because we preserve that nucleotide state by adding phalloidin to stabilize the actin (31), we use both M5 and M6 to assess the organization of both young and old actin filaments in the extracted cells.

In total, we observed 208,000 M5 paths and 134,000 M6 paths over 325 separate HCT116 cells (*SI Appendix*, Table S1 and Movies S1–S4). By tracking single myosin molecules, we identify where M5 and M6 motors land at the start of their path along the cellular actin. We mark these landing sites in green, and the intensity of the green color reflects the frequency of landing events in that area (Fig. 4*A* and see *SI Appendix*, Fig. S3*A*). For both motors, landing occurs throughout the cellular actin with some regional hot spots. We also plot the paths directly, which

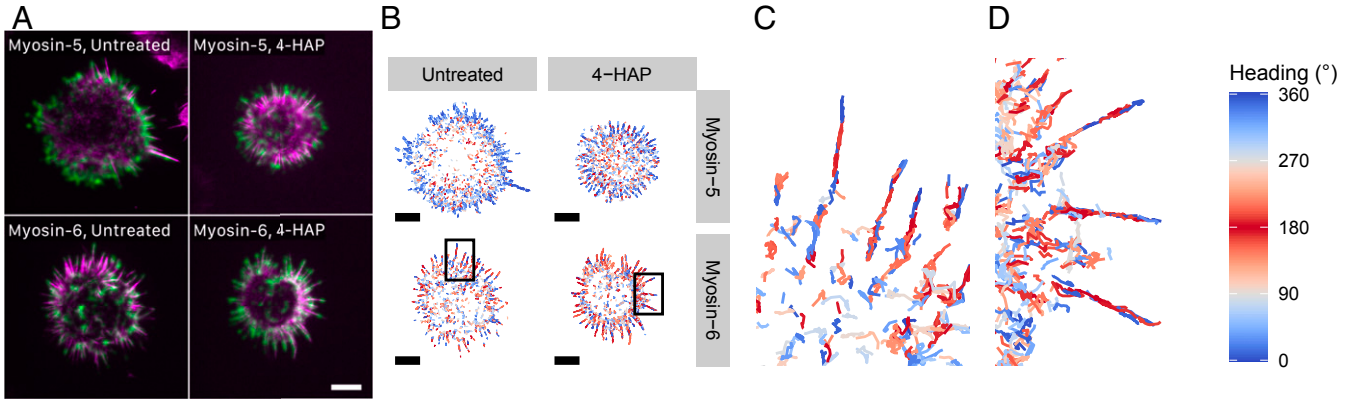

Fig. 4. Adherent HCT116 cells display mixed polarity actin filament networks. (*A*) Ex vivo motility using M5 and M6 on untreated HCT116 and 1-μM 4-HAP-treated HCT116 cells. Magenta shows the actin network visualized with TMR-phalloidin; green shows the myosin landing intensity, a kernel-density estimate of all trajectory starting points. Adherent HCT116 cells are round with numerous thin projections resembling filopodia and are apparently devoid of stress fibers. (*B*) Maps of myosin paths for the cells in (*A*), colored by their run heading relative to the cell center. On average, M5 runs out (angle 0°/360°, blue), and M6 runs in (angle 180°, red). These directions are expected for these two myosins, which travel in opposite directions along actin. However, a close inspection of the projections in untreated (*C*) and treated (*D*) cells (corresponding to the boxed regions in *B*) shows that many of the projections have mixed actin filament polarity as apparent from the presence of both red and blue trajectories for each myosin. We detected n = 1,200–1,600 runs in the cells shown here (Scale bars, 5 μm.)

produces a map of traffic along the underlying actin filaments. For each path, we calculate several metrics that characterize the motility. Here, we focus on one of these metrics, the path "heading," which reports the direction of the processive run (Fig. 4 *B* and *C* and see *SI Appendix*, Fig. S3*B*). We color the path shades of blue when the path travels away from the cell center and shades of red when the path runs toward the cell center according to the heading value. M5 is a barbed-end-directed myosin (32), and because the barbed ends of actin are typically oriented toward the cell periphery, most of the M5 paths are directed outward (blue, see *SI Appendix*, Fig. S2). M6 runs in reverse, toward the pointed end of actin (33), and therefore the M6 paths are largely directed inward (red, see *SI Appendix*, Fig. S2). Even though the apparent filopodial projections at the cell periphery follow these trends, a close examination reveals that some of these projections contain stretches with mixed filament polarity (Fig. 4*C*). This mixed filament polarity is atypical for filopodia, which contain actin nucleators and crosslinkers that enforce a uniform barbed-end-outward-directed arrangement. Thus, even though we do not see obvious contractile structures, such as stress fibers, the actin that we observe at the cell periphery is of mixed polarity and is consistent with contractile actin networks where NM2C could operate.

4-HAP Acts through NM2C to Enhance Mixed-Polarity Actin Networks. As noted above, active NM2C condenses and contracts mixed polarity actin. Therefore, actin filament polarity is one indicator of where NM2C is operating. A related indicator that we can detect using ex vivo motility is the path "persistence," which is a measure of the tendency of a single myosin path to reverse direction. A straight-line path has a high persistence, while a path with many reversals will have a low persistence. We expect that persistence values will decrease on condensed mixed-polarity networks because myosin motors can switch from one actin filament to another at actin filament intersections (34, 35).

Our example cell maps of myosin persistence show that persistence values drop upon 4-HAP treatment, an effect that is stronger for M5 than for M6 (Fig. 5*A*; note the shift from yellow toward blue upon 4-HAP treatment). When we collect persistence values over all observed cells, we find that both trends hold: M5′s persistence drops as does M6′s but to a lesser extent. Moreover, when we deplete NM2C, we abolish the 4-HAP response for M5 and reduce the response for M6 (Fig. 5*B* and see *SI Appendix*, Fig. S4). Because NM2C is only ∼5% of the total NM2 in the cell, its activation through 4-HAP affects only a small fraction of the total actin, but we are still able to detect that small fraction here. We conclude that activation of NM2C by 4-HAP promotes the formation of mixed-polarity actin networks. As part of this process, we hypothesize that NM2C slides filaments until it mechanically stalls where it would remain attached to actin. Therefore, these regions of mixed polarity would tend to trap the activated NM2C in scattered locations around the cell.

Discussion

The actomyosin cytoskeleton plays a pivotal role in the process of metastatic development and has been identified as a potential target for novel therapeutics (36–38). Cells undergo complex shape changes that are both in response to, and effectors of, metastatic pathways (39, 40). Malignant metastatic cells must adapt to a variety of mechanical environments and deform during migration through the dense surrounding matrix (11, 41, 42). NM2 controls cell shape through actin remodeling and is a key downstream player in the mediation of cellular polarity, adhesive, and contractile properties, and the development of proinvasive cellular protrusions, such as invadopodia (21). Here, we show that 4-HAP inhibits adhesion, invasion, and migration, significantly limiting the development of distant metastases in an in vivo model. This inhibition primarily occurs through NM2C as determined through a series of knockdown experiments.

Aberrant cytoskeletal regulation is a prominent feature in cancer (43, 44). Colon cancer HCT116 cells have a mutation (G13D) in one of the two alleles of the K-RAS oncogene, producing a constitutively active variant (45). Such activating K-RAS mutations are also found in ∼40% of colon cancers (46). A major consequence of K-RAS activation is that it blocks NM2 activation and stress fiber formation, even in the presence of active Rho signaling (45). Thus, the HCT116 cells have reduced actomyosin activity.

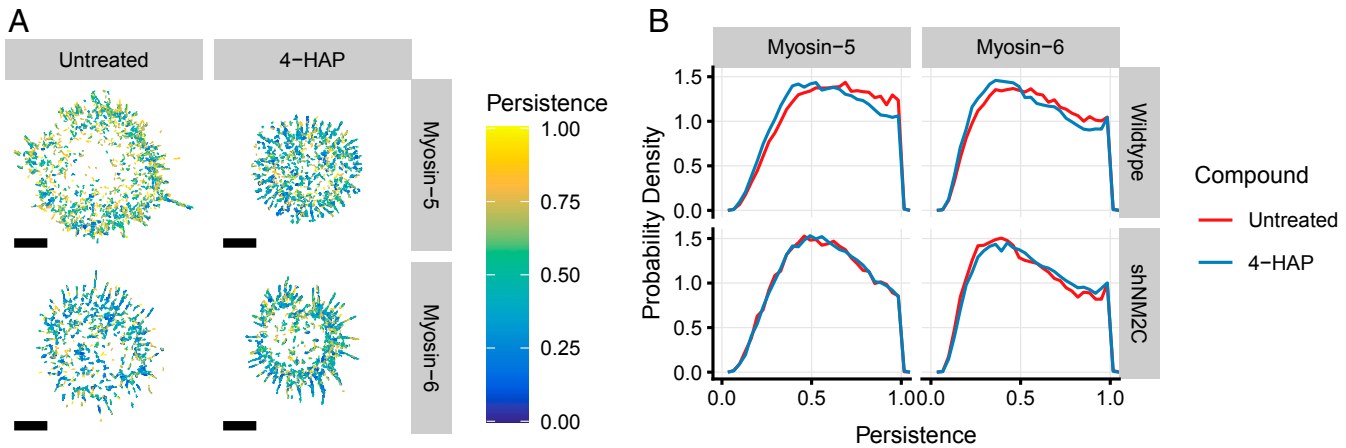

Fig. 5. Treatment with 4-HAP enhances mixed polarity actin networks required for contractility and depends on NM2C. (*A*) Maps of myosin paths of the cells in Fig. 4*A*, colored by their persistence scores. Persistence is defined as the end-to-end distance divided by the contour length of each path. The persistence value is one for a straight path and approaches zero for paths with many bends or reversals. Such reversals indicate that the myosin switched actin filaments within its run and is an indicator of mixed-polarity networks. Note the increase in the number of blue low persistence paths in the 4-HAP-treated cells. (*B*) Path persistence distributions for all 340,000 myosin paths. Treatment with 4-HAP reduces the persistence of both M5 (Kruskal–Wallis $P = 0$ and Dunn test $P < 0.0001$) and, to a lesser extent, M6 (Kruskal–Wallis $P = 0$ and Dunn test $P < 0.0001$) paths in wild type cells (top row). When NM2C is depleted (bottom row), M5 path persistence distributions are insensitive to 4-HAP treatment (Dunn test $P = 0.07$), and M6 persistence differences ±4-HAP are reduced relative to wild type (Dunn test $P < 0.0001$). We conclude that 4-HAP treatment causes actin remodeling with an increased density of mixed-polarity regions in the actin network. Our M5 and M6 probes detect these mixed-polarity regions by changing direction in a processive run, which reduces the path persistence. The activity of NM2C is the primary source of 4-HAP-dependent actin remodeling. An α level of 0.05 determined significance (Scale bars, 5 μm.)

By applying 4-HAP, NM2C condenses cortical actin into antiparallel networks. We detect these 4-HAP-mediated antiparallel networks by tracking processive myosins in the ex vivo motility assay, which is sensitive to changes in actin filament polarity and density. Remarkably, we could identify actin rearrangements from a targeted treatment that activates only 5% of the total NM2. Compared to NM2A, the NM2B and NM2C myosin isoforms spend a greater fraction of the ATPase cycle bound to actin and have load-sensitive ADP release kinetics, and are, thus, adapted to stall and remain in the rigor state on actin filaments (47–49). As a result, NM2B and NM2C may have greater contributions to cell mechanics than suggested by their abundance relative to NM2A.

One way to inhibit metastasis is to alter global mechanical properties of the cell, such as cortical tension. For example, a treatment that globally stiffens cells might overwhelm the machinery required for tumor cell invasion and migration. However, because 4-HAP's antimigration and antimetastatic activities operate through NM2C (Figs. 1 and 2) while 4-HAP's tension modulation does not (Fig. 3), we expect a more elaborate mechanism is operating in this metastasis model system. One possibility is that 4-HAP prevents dynamic relocalization of NM2C to sites where it is needed to drive cell migration. Activating NM2C traps it in scattered locations around the cell, blocking its ability to respond to chemical and mechanical signals that direct localization and assembly during metastasis. In support of this notion, Surcel has observed that 4-HAP blocks NM2C's mechanosensitive accumulation at a micropipette aspiration site in pancreatic cancer cells (24). Note that NM2A is mechanosensitive in these aspiration assays but is unaffected by 4-HAP, while NM2B is not mechanosensitive but is activated by 4-HAP (24). Thus, NM2C is the only M2 isoform which is both mechanosensitive and activated by 4-HAP. As we show here, NM2C is also the major target for 4-HAP's antimetastatic activity. We, therefore, propose that 4-HAP treatment of HCT116 cells reduces the cytoskeletal plasticity of NM2C required for migratory and invasive behaviors.

NMs have been attractive targets for numerous clinical applications, including tumor chemotherapy, neuropathy, and fibrosis (50). However, the majority of these interventions have focused on myosin inhibition strategies, largely through the small molecule blebbistatin. Here, we show that an alternative approach, targeted activation of NM2C, is effective against metastasis. This approach is a biomedical application to target NM2C (50). We expect that any malignant tumor expressing NM2C, even at low levels, would be susceptible to 4-HAP treatment.

Compounds, such as 4-HAP might be more effective antimetastatic agents than those previously investigated because they act on direct effector mechanisms that drive invasion and migration (14, 18). Here, correcting the K-RAS-induced cytoskeletal defects do not require inhibiting K-RAS itself (51). In this way, it may be possible to take advantage of biomechanical differences between cancer cells and their normal counterparts. Note that even the most effective anticancer strategy that targets the cytoskeleton is likely to be most effective when combined with therapies that help to achieve local control and decrease disease burden. Indeed, further research is needed to investigate multimodal therapy that pairs 4-HAP treatment with surgery, radiation, immunotherapy, and cytotoxic agents.

Materials and Methods

Cell Lines and Reagents. The HCT116 cell line was from the American Type Culture Collection and maintained in McCoy's 5A medium (Gibco) supplemented with 10% fetal bovine serum (Atlanta Biologicals), 100-U/mL penicillin, and 0.1-mg/mL streptomycin (Gibco). The shNM2C HCT116 cell line was generated by lentiviral infection (see *SI Appendix, SI Materials and Methods*). The 4-hydroxyacetophenone was from Sigma-Aldrich.

Proliferation, Adhesion, Invasion, and Migration Assays. Proliferation assays were performed in triplicate in 96-well plates. HCT116 cells (wild type and shNM2C) in Dulbecco's modified Eagle's medium (DMEM) were plated at a concentration of 5,000 cells per well. After 12 h, 4-HAP was added at 0, 1, 2, and 4 μM. After 24-, 48-, and 72-h incubation, media was aspirated, and CellTiter-Blue (Promega, Madison, USA) was added to the wells. After 1 h, absorbance was read at 590 nm. Adhesion assays were performed in 96-well plates coated with MatriGel Matrix (Corning). HCT116 cells in DMEM were plated at 50,000 cells per well with 4-HAP added immediately at 0, 1, 2, and 4 μM. After 8 h, media was aspirated, and CellTiter-Blue was added to the wells. After 1 h, absorbance was read at 590 nm. Invasion and migration assays were performed using Corning 8-μM pore transwell membrane inserts coated with MatriGel (invasion) or type I collagen (migration). HCT116 cells were plated at a concentration of 200,000 cells per well in the presence of 0-, 1-, 2-, and 4-μM 4-HAP. After 24 h, the transwell membranes were removed, fixed with 4% paraformaldehyde, and stained with Hoechst dye. Invaded and migrated cells were counted by fluorescence imaging.

Animal Models. Mice (6–8-wk-old female, athymic, *nude* mice) were from Envigo. The mice (n = 5 per group) underwent daily intraperitoneal (i.p.) injections with 1-mg/kg 4-HAP for 3 d. On day three, mice underwent intrasplenic injection of 1.5×10^6 HCT116 cells in 100-μL PBS, followed by splenectomy after 5 min. Cells were labeled with both TdTomato and luciferase. Mice continued to receive daily i.p. injections of 1-mg/kg 4-HAP. We performed weekly *in vivo* bioluminescent imaging to track development of liver metastases. All animal procedures were approved by the Institutional Animal Care and Use Committee at The University of Chicago and performed under sterile conditions.

Cortical Tension Measurements. Cells were treated with 500-nM 4-HAP diluted in PBS or PBS alone for 1 h, then trypsinized, and resuspended in media with or without 4-HAP. Cells were aspirated with a glass pipette, radius (R_p) of 5 to 6 μm to the equilibrium pressure (ΔP) where the length of the cell inside the pipette (L_p) was equal to R_p. Because shCtrl cells treated with 4-HAP were susceptible to blebbing, we reduced the rate of the pressure ramp for both untreated and treated cells to allow distortion of the cell cortex without blebbing. The effective cortical tension (T_{eff}) was calculated by applying the Young–Laplace equation: $\Delta P = 2T_{eff}\,(1/R_p - 1/R_c)$ where R_c is the radius of the cell and ΔP is the equilibrium pressure when $L_p = R_p$. Images were collected with an Olympus IX81 microscope equipped with MetaMorph software and analyzed using ImageJ (https://imagej.nih.gov/ij/).

Ex Vivo Motility. HCT116 cells were plated on polylysine-coated glass coverslips, extracted with detergent to remove the plasma membrane and imaged with myosin motors in a single-molecule format as described by Brawley et al. (29) with modifications described in the *SI Appendix, SI Materials and Methods*. Myosin tracking was automated using custom software (*SI Appendix*).

For additional experimental details for all experiments, see the *SI Appendix, SI Materials and Methods*.

Data Availability. All study data are included in the article and *SI Appendix*.

ACKNOWLEDGMENTS. We acknowledge the University of Chicago Research Computing Center for support of this work. This work was supported by NIH Grant R01 GM109863 (to D.N.R. and R.S.R.); NIH Grant R01 GM124272 (to R.S.R.); a Cancer Center Support Grant P30CA014599, the Ludwig Foundation, a gift from the Foglia Foundation (to R.R.W.), and a Johns Hopkins Discovery Grant (to D.N.R.).

1. R. L. Siegel, K. D. Miller, A. Jemal, Cancer statistics, 2016. *CA Cancer J. Clin.* **66**, 7–30 (2016).
2. N. Howlader *et al.*, *SEER Cancer Statistics Review, 1975-2013*, (National Cancer Institute, Bethesda, MD, 2016).
3. S. Hellman, R. R. Weichselbaum, Oligometastases. *J. Clin. Oncol.* **13**, 8–10 (1995).
4. M. K. H. Hong *et al.*, Tracking the origins and drivers of subclonal metastatic expansion in prostate cancer. *Nat. Commun.* **6**, 6605 (2015).
5. M.-Y. Kim *et al.*, Tumor self-seeding by circulating cancer cells. *Cell* **139**, 1315–1326 (2009).
6. J. Massagué, E. Batlle, R. R. Gomis, Understanding the molecular mechanisms driving metastasis. *Mol. Oncol.* **11**, 3–4 (2017).
7. C. H. Stuelten, C. A. Parent, D. J. Montell, Cell motility in cancer invasion and metastasis: Insights from simple model organisms. *Nat. Rev. Cancer* **18**, 296–312 (2018).
8. V. Marx, Tracking metastasis and tricking cancer. *Nature* **494**, 133–136 (2013).

9. G. P. Gupta, J. Massagué, Cancer metastasis: Building a framework. *Cell* **127**, 679–695 (2006).
10. D. Hanahan, R. A. Weinberg, Hallmarks of cancer: The next generation. *Cell* **144**, 646–674 (2011).
11. D. Wirtz, K. Konstantopoulos, P. C. Searson, The physics of cancer: The role of physical interactions and mechanical forces in metastasis. *Nat. Rev. Cancer* **11**, 512–522 (2011).
12. P. S. Steeg, Tumor metastasis: Mechanistic insights and clinical challenges. *Nat. Med.* **12**, 895–904 (2006).
13. I. J. Fidler, The pathogenesis of cancer metastasis: The "seed and soil" hypothesis revisited. *Nat. Rev. Cancer* **3**, 453–458 (2003).
14. A. Gandalovičová *et al*., Migrastatics-anti-metastatic and anti-invasion drugs: Promises and challenges. *Trends Cancer* **3**, 391–406 (2017).
15. V. Sanz-Moreno *et al*., Rac activation and inactivation control plasticity of tumor cell movement. *Cell* **135**, 510–523 (2008).
16. V. Sanz-Moreno, C. J. Marshall, The plasticity of cytoskeletal dynamics underlying neoplastic cell migration. *Curr. Opin. Cell Biol.* **22**, 690–696 (2010).
17. V. te Boekhorst, P. Friedl, "Chapter seven–Plasticity of cancer cell invasion—Mechanisms and implications for therapy" in *Advances in Cancer Research*, D. R. Welch, P. B. Fisher, Eds. (Academic Press, 2016), Vol. 132, pp. 209–264.
18. S. Ivkovic *et al*., Direct inhibition of myosin II effectively blocks glioma invasion in the presence of multiple motogens. *Mol. Biol. Cell* **23**, 533–542 (2012).
19. M. Vicente-Manzanares, J. Zareno, L. Whitmore, C. K. Choi, A. F. Horwitz, Regulation of protrusion, adhesion dynamics, and polarity by myosins IIA and IIB in migrating cells. *J. Cell Biol.* **176**, 573–580 (2007).
20. M. Vicente-Manzanares, M. A. Koach, L. Whitmore, M. L. Lamers, A. F. Horwitz, Segregation and activation of myosin IIB creates a rear in migrating cells. *J. Cell Biol.* **183**, 543–554 (2008).
21. M. Vicente-Manzanares, X. Ma, R. S. Adelstein, A. R. Horwitz, Non-muscle myosin II takes centre stage in cell adhesion and migration. *Nat. Rev. Mol. Cell Biol.* **10**, 778–790 (2009).
22. R. Aguilar-Cuenca, A. Juanes-García, M. Vicente-Manzanares, Myosin II in mechanotransduction: Master and commander of cell migration, morphogenesis, and cancer. *Cell. Mol. Life Sci.* **71**, 479–492 (2014).
23. A. Surcel *et al*., Pharmacological activation of myosin II paralogs to correct cell mechanics defects. *Proc. Natl. Acad. Sci. U.S.A.* **112**, 1428–1433 (2015).
24. A. Surcel *et al*., Targeting mechanoresponsive proteins in pancreatic cancer: 4-Hydroxyacetophenone blocks dissemination and invasion by activating MYH14. *Cancer Res.* **79**, 4665–4678 (2019).
25. G. Oshima *et al*., Advanced animal model of colorectal metastasis in liver: imaging techniques and properties of metastatic clones. *J. Visualized Exp.* **117**, 54657 (2016).
26. E. M. Reichl *et al*., Interactions between myosin and actin crosslinkers control cytokinesis contractility dynamics and mechanics. *Curr. Biol.* **18**, 471–480 (2008).
27. L. Blanchoin, R. Boujemaa-Paterski, C. Sykes, J. Plastino, Actin dynamics, architecture, and mechanics in cell motility. *Physiol. Rev.* **94**, 235–263 (2014).
28. A. C. Reymann *et al*., Actin network architecture can determine myosin motor activity. *Science* **336**, 1310–1314 (2012).
29. C. M. Brawley, R. S. Rock, Unconventional myosin traffic in cells reveals a selective actin cytoskeleton. *Proc. Natl. Acad. Sci. U.S.A.* **106**, 9685–9690 (2009).
30. S. Brown, W. Levinson, J. A. Spudich, Cytoskeletal elements of chick embryo fibroblasts revealed by detergent extraction. *J. Supramol. Struct.* **5**, 119–130 (1976).
31. D. Zimmermann, A. Santos, D. R. Kovar, R. S. Rock, Actin age orchestrates myosin-5 and myosin-6 run lengths. *Curr. Biol.* **25**, 2057–2062 (2015).
32. R. E. Cheney *et al*., Brain myosin-V is a two-headed unconventional myosin with motor activity. *Cell* **75**, 13–23 (1993).
33. A. L. Wells *et al*., Myosin VI is an actin-based motor that moves backwards. *Nature* **401**, 505–508 (1999).
34. M. Y. Ali *et al*., Myosin Va maneuvers through actin intersections and diffuses along microtubules. *Proc. Natl. Acad. Sci. U.S.A.* **104**, 4332–4336 (2007).
35. M. Y. Ali, S. B. Previs, K. M. Trybus, H. L. Sweeney, D. M. Warshaw, Myosin VI has a one track mind versus myosin Va when moving on actin bundles or at an intersection. *Traffic* **14**, 70–81 (2013).
36. R. A. Patel, Y. Liu, B. Wang, R. Li, S. M. Sebti, Identification of novel ROCK inhibitors with anti-migratory and anti-invasive activities. *Oncogene* **33**, 550–555 (2014).
37. J. E. Talmadge, I. J. Fidler, AACR centennial series: The biology of cancer metastasis: Historical perspective. *Cancer Res.* **70**, 5649–5669 (2010).
38. C. M. Fife, J. A. McCarroll, M. Kavallaris, Movers and shakers: Cell cytoskeleton in cancer metastasis. *Br. J. Pharmacol.* **171**, 5507–5523 (2014).
39. P. Pandya, J. L. Orgaz, V. Sanz-Moreno, Actomyosin contractility and collective migration: May the force be with you. *Curr. Opin. Cell Biol.* **48**, 87–96 (2017).
40. S. C. Wei *et al*., Matrix stiffness drives epithelial-mesenchymal transition and tumour metastasis through a TWIST1-G3BP2 mechanotransduction pathway. *Nat. Cell Biol.* **17**, 678–688 (2015).
41. J. Guck *et al*., Optical deformability as an inherent cell marker for testing malignant transformation and metastatic competence. *Biophys. J.* **88**, 3689–3698 (2005).
42. S. Suresh *et al*., Connections between single-cell biomechanics and human disease states: Gastrointestinal cancer and malaria. *Acta Biomater.* **1**, 15–30 (2005).
43. T. Takaki *et al*., Actomyosin drives cancer cell nuclear dysmorphia and threatens genome stability. *Nat. Commun.* **8**, 16013 (2017).
44. D. B. Agus *et al*.; Physical Sciences–Oncology Centers Network, A physical sciences network characterization of non-tumorigenic and metastatic cells. *Sci. Rep.* **3**, 1449 (2013).
45. C. B. Pollock, S. Shirasawa, T. Sasazuki, W. Kolch, A. S. Dhillon, Oncogenic K-RAS is required to maintain changes in cytoskeletal organization, adhesion, and motility in colon cancer cells. *Cancer Res.* **65**, 1244–1250 (2005).
46. J. L. Bos *et al*., Prevalence of ras gene mutations in human colorectal cancers. *Nature* **327**, 293–297 (1987).
47. M. Kovács, K. Thirumurugan, P. J. Knight, J. R. Sellers, Load-dependent mechanism of nonmuscle myosin 2. *Proc. Natl. Acad. Sci. U.S.A.* **104**, 9994–9999 (2007).
48. M. F. Norstrom, P. A. Smithback, R. S. Rock, Unconventional processive mechanics of non-muscle myosin IIB. *J. Biol. Chem.* **285**, 26326–26334 (2010).
49. K. Chinthalapudi, S. M. Heissler, M. Preller, J. R. Sellers, D. J. Manstein, Mechanistic insights into the active site and allosteric communication pathways in human nonmuscle myosin-2C. *eLife* **6**, e32742 (2017).
50. A. Á. Rauscher, M. Gyimesi, M. Kovács, A. Málnási-Csizmadia, Targeting myosin by blebbistatin derivatives: Optimization and pharmacological potential. *Trends Biochem. Sci.* **43**, 700–713 (2018).
51. Q. Sun *et al*., Competition between human cells by entosis. *Cell Res.* **24**, 1299–1310 (2014).